Journal of Neuroscience Methods 274 (2016) 27–37

Contents lists available at ScienceDirect

Journal of Neuroscience Methods

journal homepage: www.elsevier.com/locate/jneumeth

Real-time EEG artifact correction during fMRI using ICA

Ahmad Mayeli[a,b], Vadim Zotev[a], Hazem Refai[b], Jerzy Bodurka[a,c,d,*]

[a] Laureate Institute for Brain Research, Tulsa, OK, USA
[b] Department of Electrical and Computer Engineering, University of Oklahoma, Tulsa, OK, USA
[c] Stephenson School of Biomedical Engineering, University of Oklahoma, Norman, OK, USA
[d] Biomedical Engineering Center, University of Oklahoma, Norman, OK, USA

HIGHLIGHTS

- A real-time method based on ICA (rtICA) is proposed to remove artifacts from EEG data acquired simultaneously with fMRI.
- The rtICA effectively reduces ocular, motion, BCG, muscle and residual MR artifacts and retrieves EEG signals.
- The rtICA method following the rtAAS outperforms the rtAAS for removing artifacts in real time.
- The rtICA revealed reliable artifact suppression results for further applications of real-time multimodal EEG-fMRI.

ARTICLE INFO

Article history:
Received 18 July 2016
Received in revised form 8 September 2016
Accepted 29 September 2016
Available online 30 September 2016

Keywords:
Real-time artifact correction
fMRI
EEG
EEG-fMRI
Real-time ICA

ABSTRACT

Background: Simultaneous acquisition of EEG and fMRI data results in EEG signal contamination by imaging (MR) and ballistocardiogram (BCG) artifacts. Artifact correction of EEG data for real-time applications, such as neurofeedback studies, is the subject of ongoing research. To date, average artifact subtraction (AAS) is the most widespread real-time method used to partially remove BCG and imaging artifacts without requiring extra hardware equipment; no alternative software-only real time methods for removing EEG artifacts are available.

New methods: We introduce a novel, improved approach for real-time EEG artifact correction during fMRI (rtICA). The rtICA is based on real time independent component analysis (ICA) and it is employed following the AAS method. The rtICA was implemented and validated during EEG and fMRI experiments on healthy subjects.

Results: Our results demonstrate that the rtICA employed after the rtAAS can obtain 98.4% success in detection of eye blinks, 4.4 times larger INPS reductions compared to RecView-corrected data, and effectively reduce motion artifacts, as well as imaging and muscle artifacts, in real time on six healthy subjects.

Comparison with existing methods: We compared our real-time artifact reduction results with the rtAAS and various offline methods using multiple evaluation metrics, including power analysis. Importantly, the rtICA does not affect brain neuronal signals as reflected in EEG bands of interest, including the alpha band.

Conclusions: A novel real-time ICA method was proposed for improving the EEG quality signal recorded during fMRI acquisition. The results show substantial reduction of different types of artifacts using real-time ICA method.

1. Introduction

Electroencephalography (EEG) and functional Magnetic Resonance Imaging (fMRI) are widely used, noninvasive, and safe techniques for detecting and characterizing changes in brain states and their relation to brain activity (Ritter and Villringer, 2006). The techniques complement each other well because of high temporal resolution of EEG data and high spatial resolution of fMRI data (Niazy et al., 2005). Furthermore, because EEG is a direct measure of brain activity and fMRI is an indirect measure, simultaneous EEG-fMRI measurements can aid in cross validation. However, recording EEG inside the MRI scanner and during fMRI acquisition suffers from several safety and technical challenges (Kruggel et al., 2000). A major problem is the presence of artifacts in EEG data, such as MR or imaging artifacts and also ballistocardiogram (BCG) artifacts. BCG and imaging artifacts appear in the EEG signal as a result of the sig-

* Corresponding author at: Laureate Institute for Brain Research, Tulsa, OK, USA.
E-mail address: jbodurka@laureateinstitute.org (J. Bodurka).

http://dx.doi.org/10.1016/j.jneumeth.2016.09.012

nal being recorded inside MRI scanner and during fMRI acquisition respectively (Niazy et al., 2005). Other types of artifacts, such as muscle and ocular artifacts can be present in EEG data regardless if the EEG is recorded inside or outside the MRI scanner (Mantini et al., 2007; McMenamin et al., 2010).

The average artifact subtraction method (AAS) (Allen et al., 1998, 2000) is commonly used to remove BCG and imaging artifacts. To date, it is the most widespread real-time method used to partially remove such artifacts. The AAS method is based on the repetitive pattern of imaging and BCG artifacts, and it generates an artifact template to subtract it from the EEG signal. Even though the AAS can effectively reduce BCG and imaging artifacts, some residual artifacts remain when this algorithm is applied to raw EEG data in both real time and offline (Niazy et al., 2005). High quality, modern MRI scanner gradient controllers together with synchronization of MRI and EEG system clocks enable generation of accurate and reproducible templates of gradient artifacts, and allow for AAS template subtraction that has proven extremely successful (Laufs, 2012). However, temporal variability of BCG artifact makes removal of BCG artifact using the AAS less efficient. While the AAS has proven successful for reducing BCG and, especially, imaging artifacts, the method does not remove ocular, motion, and muscle artifacts. Instead, ICA has been widely used in offline analysis as an alternative for attenuating residual imaging and BCG artifacts, and other artifacts (e.g., Mantini et al., 2007; McMenamin et al., 2010; Srivastava et al., 2005; Wong et al., 2016; Zotev et al., 2016). A variety of ICA-based methods (e.g., FastICA, extended Infomax, Robust ICA, JADE, and SOBI) have been utilized for this purpose. More recently, Hsu et al. (2016) demonstrated that online recursive ICA algorithms are fast enough for real-time EEG source separation. However, they did not suggest any automatic algorithm for identifying artifacts among sources in their study.

Problems associated with EEG artifacts have led to the development of a number of alternative methods for removing fMRI environment and regular physiological artifacts. Niazy et al. (2005) suggested a novel method, namely optimal basis set (OBS), for generating BCG artifact templates. They used principal component analysis (PCA) for capturing temporal variations in artifacts and regressing BCG artifacts from EEG data. The result is superior performance over the AAS for removing BCG artifacts, with fewer residual artifacts remaining. This method has recently been adopted for real-time artifact correction (Wu et al., 2016). Like the rtAAS, this method can only remove BCG and imaging artifacts and the application of this method is obscured when the accuracy of R-peak detection is low due to ECG data distortion. Furthermore, since muscle and especially ocular and motion artifacts often have greater amplitudes compared to neural activity and higher or similar amplitude to BCG artifacts, the interaction of motion, muscle and ocular artifacts on BCG artifact template needs to be investigated further (Wu et al., 2016). Kim et al. (2004) proposed a combination of wavelet-based de-noising with adaptive filtering as post-processing to increase the AAS performance. Likewise, adaptive noise cancellation was suggested as a preprocessing step for the OBS (Niazy et al., 2005). PCA has also been used for removing BCG and imaging artifacts in studies reported in Negishi et al. (2004) and Bénar et al. (2003). Wavelet transform, followed by ICA, has proven to be a useful method for removing artifacts (Akhtar et al., 2012; Zhou and Gotman, 2004).

Several researchers utilized reference signals for removing BCG artifacts (Bonmassar et al., 2002; Dunseath and Alden, 2010; Luo et al., 2014; Masterton et al., 2007; van der Meer et al., 2016). Bonmassar et al. (2002) utilized a piezoelectric motion sensor to estimate motion artifact noise. Correlation between motion sensor and EEG signal was used to design the Kalman filter for removing BCG artifacts. Masterton et al. (2007) introduced a wire-loop-based method for correction of motion and BCG artifacts. Dunseath and Alden (2010) suggested using reference electrodes attached to a conductive reference layer for recording artifacts and further removing noise from EEG data. Although these methods appear beneficial for reducing artifacts, they are not yet widely used. Unfortunately, these methods require hardware modification and additional equipment, which makes them complicated and more expensive to implement (Jorge et al., 2015). Furthermore, some of these methods require complicated and time consuming calculations, which make them less suitable for real-time applications.

Real-time imaging and BCG artifact correction techniques were used in several simultaneous EEG and fMRI studies (Becker et al., 2011; Cavazza et al., 2014; Zich et al., 2015; Zotev et al., 2014). The AAS implemented in real time in the RecView software (Brain Products GmbH, Gilching, Germany) was used in all of these studies for reducing BCG and imaging artifacts. Developing new real-time algorithms for removing EEG artifacts would make real-time analysis of multimodal EEG-fMRI signals more feasible and thus open many new research opportunities to study human brain function.

In this work, a novel real-time EEG artifact correction approach during fMRI (rtICA) is developed. The rtICA is a real-time ICA-based algorithm for reducing BCG and imaging artifacts, in addition to motion, ocular, and muscle EEG artifacts, and to improve EEG data quality acquired during fMRI. Imaging and BCG artifacts are first reduced using the BrainVision RecView software in real time prior to applying the rtICA (rtAAS + rtICA). The following section provides a more detailed description of our proposed rtICA method. Since the EEG activity is changing during time and in different conditions, instead of comparing EEG data recorded during fMRI acquisition and outside MRI scanner, we preferred to compare the performance of the rtAAS + rtICA for removing artifacts with RecView-corrected data and EEG data after applying different offline artifact corrections. Finally, we discuss results and improvement of the EEG data quality. A preliminary report of portions of this work was presented in Mayeli et al. (2015).

2. Methods

2.1. Data acquisition

The study was conducted at the Laureate Institute for Brain Research with research protocol approved by the Western Institutional Review Board (IRB). All participants provided written informed consent and received financial compensation for participation.

The rtAAS + rtICA artifact removal method has been tested on six healthy subjects (mean age: 36 ± 14 years, three females). Four resting EEG-fMRI runs were conducted; each run lasted 8 min 40 s. The participants were instructed to relax and rest with eyes closed for two runs, and then keep their eyes open and fixed on a cross for an additional two runs. Sequence runs with eyes-closed and eyes-open was balanced to eliminate fatigue factor (Yuan et al., 2013).

MR images were acquired via a General Electric Discovery MR750 whole-body 3 T MRI scanner with a standard 8-channel, receive-only head coil array. For fMRI acquisition, a single-shot gradient-recalled EPI sequence with Sensitivity Encoding (SENSE) was employed. The EPI sequence was custom modified to ensure that the repetition time TR was exactly 2000 ms (with 1 μs accuracy) and further enabling accurate correction of MR artifacts in EEG data, recorded simultaneously with fMRI. EPI imaging had the following parameters: FOV = 240 mm, slice thickness = 2.9 mm, slice gap = 0.5 mm, 34 axial slices per volume, 64×64 acquisition matrix, echo time TE = 30 ms, SENSE acceleration factor R = 2, flip angle = 90°, sampling bandwidth = 250 kHz. The fMRI run time was 8 min 40 s. For allowing the fMRI signal to reach

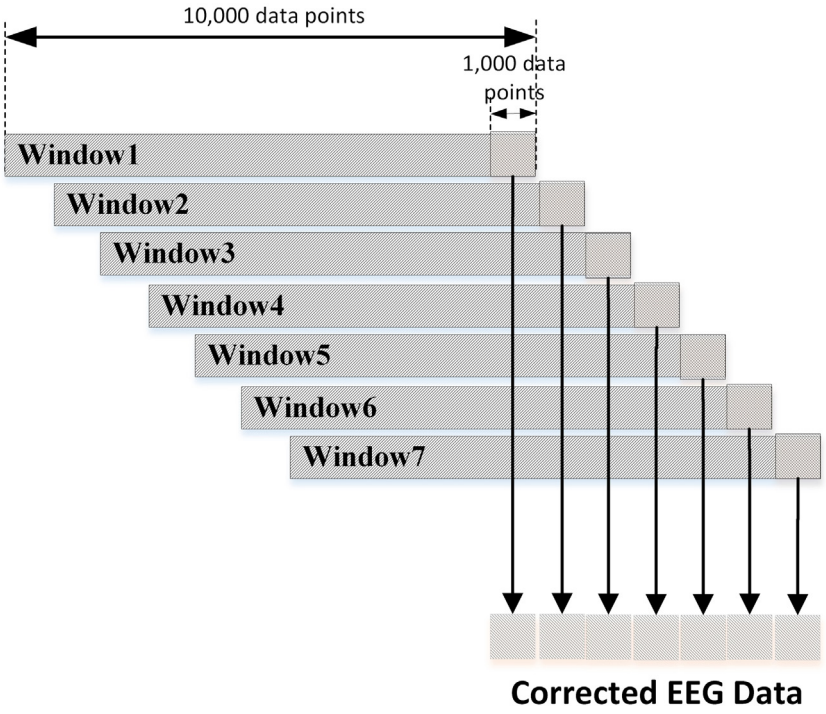

Fig. 1. Proposed data processing procedure suitable for real-time implementation. SOBI was applied on the whole 10,000 point sliding window, but the correction was only performed on the final 1000 pts.

steady state, three EPI volumes (6 s) were added at the beginning of the run and were excluded from data analysis. The fMRI voxel size was $3.75 \times 3.75 \times 2.9\,mm^3$. For acquiring anatomical image, a T1-weighted magnetization-prepared rapid gradient-echo (MPRAGE) sequence with SENSE was used. The MPRAGE sequence had the following parameters: FOV = 240 mm, axial slices per slab = 128, slice thickness = 1.2 mm, image matrix size = 256 × 256, TR/TE = 5.0/1.9 ms, SENSE factor R = 2, flip angle = 10°, delay time TD = 1400 ms, inversion time TI = 725 ms, sampling bandwidth = 31.2 kHz, scan time = 4 min 58 s.

EEG signals were recorded simultaneously with fMRI via a 32-channel MR-compatible EEG system from Brain Products GmbH. The EEG cap included 32 electrodes, arranged according to the international 10–20 system. One electrode was placed on the subject's back for recording the ECG signal. A Brain Products' SyncBox device was used to synchronize the EEG system clock with the 10 MHz MRI scanner clock. EEG acquisition temporal resolution was 0.2 ms (i.e., 16-bit 5 kS/s sampling), and measurement resolution was 0.1 μV. EEG signals were hardware filtered throughout the acquisition in a frequency band between 0.016 and 250 Hz. Brain Products' RecView software was used to monitor EEG data acquisition in real time and to reduce imaging and BCG artifacts before streaming to the rtICA module.

2.2. Second order blind identification

Second order blind identification (SOBI) (Belouchrani et al., 1997) takes advantage of temporal correlations in the source activities. It calculates second order statistics–covariance matrices–which are later diagonalized. The SOBI differs from other blind separation algorithms by its robustness, the low number of tunable parameters requiring adjustment, and convergence speed, which is the most important reason for choosing this ICA algorithm for this study. Table 1 presents the average computation time required for ICA decomposition of 40 s 22-channel data using different ICA algorithms, computed by averaging the execution time for 3 subjects during an 8 min and 40 s resting state run. The ICA computations were performed on MATLAB 2012. The ICA MATLAB codes available in EEGLAB toolbox and their default values for ICA convergence were utilized. Among the presented four algorithms, SOBI has the lowest averaged time and standard deviation. Based on Klemm et al. (2009) study comparing ICA algorithms, the SOBI has been shown to provide some of the best-quality results in separating EEG data and artifacts.

Table 1
Average computation time (s) for 40 s (10,000 data points) 22- channel data using different ICA algorithms.

	Time(s)
Infomax	13.56 ± 1.23
JADE	2.96 ± 1.28
FastICA	6.74 ± 4.54
SOBI	0.71 ± 0.10

2.3. Proposed ICA data processing suitable for real-time implementation

The proposed data processing procedure suitable for real-time implementation is shown in Fig. 1 (Mayeli et al., 2015). To obtain reliable and stable results from ICA decomposition, data submitted to the algorithm should be at least a multiple k of n^2, where n is the number of channels and k may need to be 20 or larger (Onton et al., 2006). For instance, given 31-channel data and $k = 20$, data samples will be at least 19,220. At a sampling rate of 250 S/s, data window duration is approximately 80 s. In this study, 22 channels were selected to increase algorithm speed, as opposed to performing ICA on all channels. When $n = 22$ and $k = 20$, the number of data points submitted to ICA should be more than 9680 – rounded up to 10,000 – data points. The selected channels, shown in Fig. 2, include all the available frontal EEG channels, because EEG activity over the frontal and prefrontal brain regions is relevant to emotion regulation and is used for neurofeedback studies (Cavazza et al.,

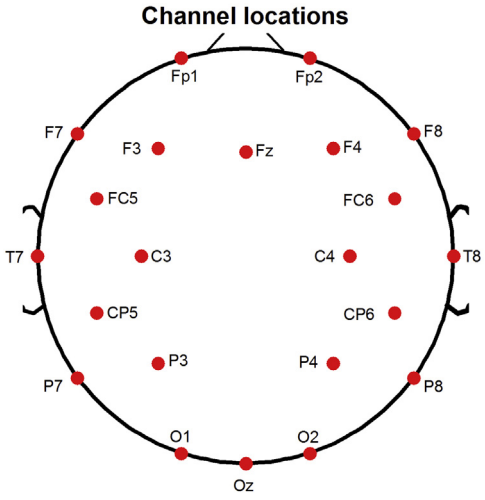

Fig. 2. Selected 22 channels for ICA decomposition.

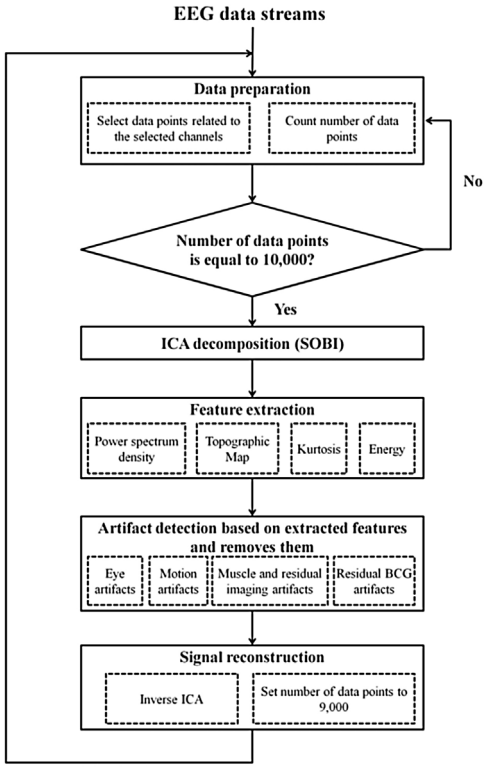

Fig. 3. rtAAS + rtICA flowchart.

2014; Zotev et al., 2014, 2016). Occipital electrodes (i.e. O1, O2 and Oz), which are important for investigating human visual evoked potential, were selected for ICA decomposition as well (Becker et al., 2008, 2011). The other channels were selected based on two criteria. First, since the BCG artifacts mostly exhibit bipolar properties, we selected symmetric channels for ICA decomposition. Second, the channels which are contaminated with artifacts and have common artifacts with occipital or frontal electrodes (e.g. channels T1 and T2 are affected by muscle artifacts) were selected. These selected channels and number of channels can be changed based on the application of real-time EEG-fMRI study and number of EEG system electrodes.

Fig. 3 offers a detailed flow diagram description of the rtAAS + rtICA process. The SOBI algorithm was implemented in the following way. The RecView software was utilized to reduce imaging and BCG artifacts from the 32-channel EEG data in real time, and then to down-sample data to 250 S/s from 5000 S/s. RecView output data were exported in 8 ms blocks (i.e., two data points per block for all channels). The number of data points is first initialized to zero. During preprocessing, newly arriving data points are counted. Since this scheme requires 23 channels (i.e., 22 EEG channels plus 1 ECG electrode) for ICA decomposition, data points related to these channels are selected. ICA decomposition commences when total number of data points reaches 10,000. Four features (power spectrum density, topographic map, kurtosis, energy) are extracted from the last 1000 data points of each independent component (IC). Based on extracted features and defined thresholds, a maximum of 12 ICs for various types of artifacts are considered (i.e., a maximum of three components for ocular, three for motion, three for muscle and residual imaging artifact, and three components for BCG artifact). The number of ICs identified as artifacts was limited to prevent losing any brain activity. After subtracting artifactual ICs, inverse ICA reconstructs EEG data, and the number of data points is set to 9000. This procedure is repeated for each 1000 data samples received.

An example application of real-time EEG acquisition is EEG neurofeedback. Frontal EEG asymmetry is a promising target for EEG neurofeedback aimed at training emotion regulation, as confirmed by recent simultaneous EEG-fMRI studies (Cavazza et al., 2014; Zotev et al., 2014, 2016). When used as a real-time target for EEG neurofeedback, frontal EEG asymmetry in a specific EEG band is defined as Zotev et al. (2014):

$$\boldsymbol{A} = \frac{[\boldsymbol{P}(\boldsymbol{F}3) - \boldsymbol{P}(\boldsymbol{F}4)]}{[\boldsymbol{P}(\boldsymbol{F}3) + \boldsymbol{P}(\boldsymbol{F}4)]} \quad (1)$$

where P is the EEG power for a given channel in a specific EEG band such as high-beta or alpha bands. Frontal EEG asymmetry in the alpha EEG band is defined with the opposite sign (Cavazza et al., 2014; Zotev et al., 2016).

2.4. Automatic IC classification

Various features are extracted from ICs and used to classify ICs as brain activity and artifacts. The first is the topographic map of each independent component, which indicates scalp map projection of selected components (i.e., each component primarily affecting a specific portion of the brain and can be determined using an ICA mixture matrix). The values of the topographic map were normalized to unity using inverse ICA matrices. The second feature is IC energy. The energy of a discrete time signal of x is defined by:

$$E_x \triangleq \sum\nolimits_{n=-\infty}^{\infty} |x[n]|^2 \quad (2)$$

Kurtosis can also be used for separating artifacts and it is a measure of data distribution (i.e., peakedness or flatness) that can be calculated using the following equation:

$$kurt(x) = E\left\{x^4\right\} - 3\left(E\left\{x^2\right\}\right)^2 \quad (3)$$

The final feature is power spectral density of IC calculated via the Fast Fourier Transform (FFT) to indicate distribution of signal power in frequency domain. For detecting eye, motion and residual BCG artifacts, the spectrum in the range between 0.5 and 40 Hz was normalized to the range of 0–1 and for detecting muscle and residual MR artifact, the spectrum in the range between 0.5 and 60 Hz was normalized to the unity.

The EEG data were recorded from three healthy female subjects (mean age: 26 ± 6 years) and three male subjects (mean age: 29 ± 9 years) diagnosed with combat related post-traumatic stress disorder (PTSD) across a neurofeedback experiment (3640 s) and were used to define a reliable threshold for each feature and to avoid removing brain activity instead of artifacts (Zotev et al., 2014).

Table 2
The summary of the identification of the ICs based on energy, kurtosis, topographic features and spectrum characteristics.

Types of Artifacts	Energy	Kurtosis	Topographic Features	Spectral Characteristics
Eye Artifacts	$>10^8$	>6	Prefrontal region (Fp1 and Fp2) with a larger threshold value of 28%	Normalized power between 0.5 and 3 Hz >0.22
Residual BCG Artifacts	–	–	Bipolar with the threshold value of larger than 0.25 AND Occipital region with a smaller threshold value of 14%	Normalized power between 2 and 7 Hz> 0.18 AND Normalized power between 7 and 12 Hz <0.12
Muscle and Residual Imaging Artifacts	–	–	Unipolar	Normalized power between 30 and 60 Hz >0.68 AND Normalized power between 7 and 12 Hz <0.07
Motion Artifacts	$>10^9$	>15	Bipolar with the threshold value of 0.2	Normalized power between 0.5 and 4.5 Hz >0.26

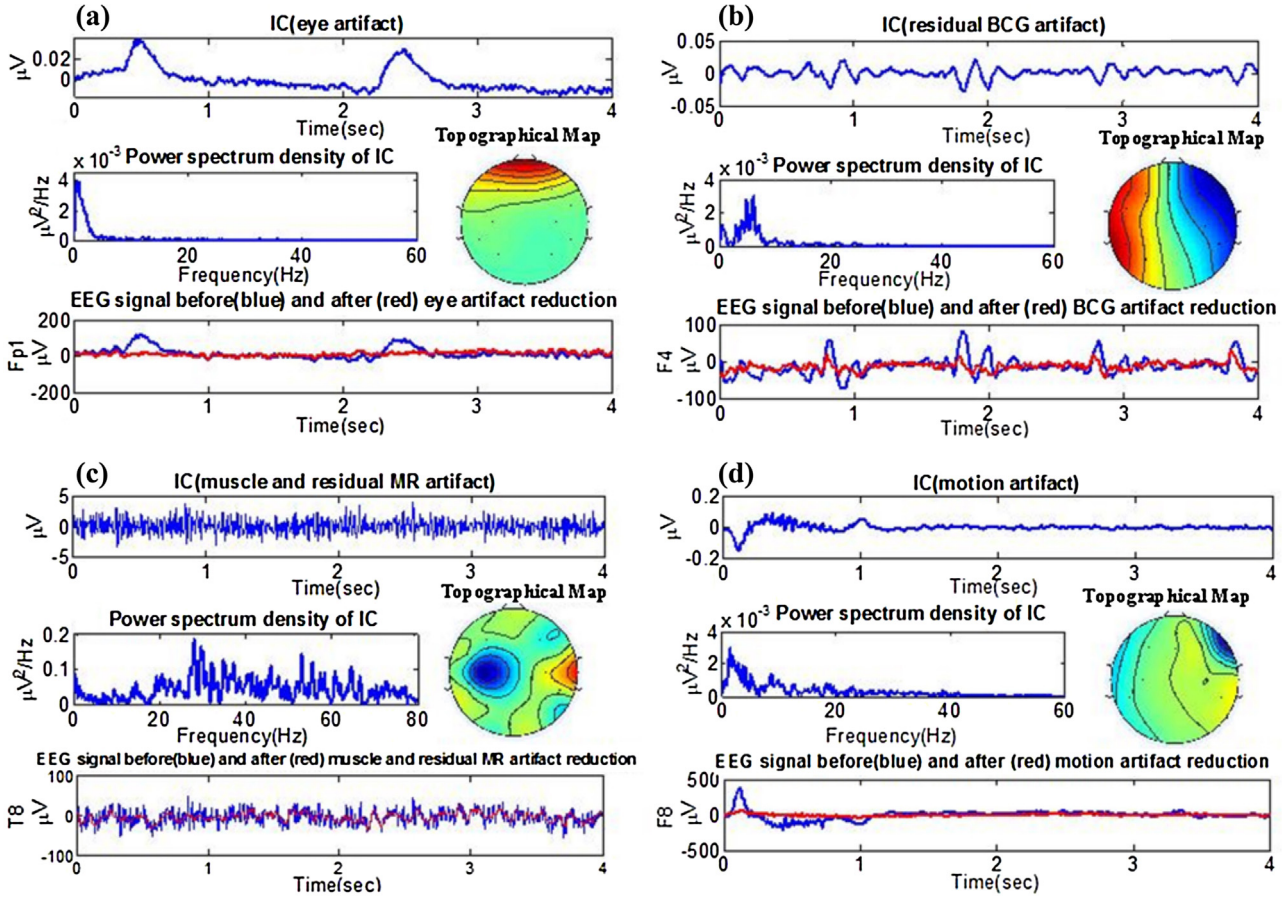

Fig. 4. Automatic (a) eye artifact, (b) residual BCG artifact, (c) residual MR and Muscle artifact and (d) motion artifact detection and results of removing them from EEG data.

Table 2 summarizes real-time classification criteria for each type of artifacts being detected including numerical threshold values for kurtosis, energy, topographic features and spectral characteristics. The described criteria are preliminary and need further optimization. Fig. 4 shows an overview of automatic artifact IC identification.

2.4.1. Eye artifact detection

Eye movement and blinking produces an electrical potential at a magnitude larger than brain activity. Due to eye proximity, ocular artifacts mostly affect frontal pole electrodes (i.e. channels Fp1 and Fp2), although they can propagate across much of the head and distort brain signals. Ocular artifacts are characterized by strong spatial projection in the prefrontal area, either shows high loadings at the most anterior sites for eye blinks or manifests as an anterior dipole for saccades, high energy and low-frequency peaks (between 0.5 and 3 Hz) in the frequency domain (McMenamin et al., 2010; Wong et al., 2016). Based on such features, ocular artifacts can be easily detected among different ICs.

2.4.2. Residual BCG artifacts detection

BCG artifacts are extremely problematic in EEG due to their overlap with frequency range of normal neural activity. Although the RecView is often used to partially remove BCG artifacts, remaining residual artifacts can obscure the EEG signal because: (1) ECG signal recorded via chest or back electrodes during fMRI contains artifacts that can make reliable R-peak detection difficult (Luo et al.,

2014); and (2) AAS algorithm assumes pulse waveform with a highly reproducible pattern within a given time interval. In this way, subtracting average waveform from contaminated EEG can appropriately remove BCG artifacts. Notably, this assumption has not been proven (Kim et al., 2004). To reduce such artifacts, IC features (e.g., high relative power of theta band activity between 2 and 7 Hz) related to BCG artifacts can be leveraged (Wong et al., 2016). Furthermore, topographical maps corresponding to residual BCG artifacts exhibit primarily bipolar properties (Zotev et al., 2012). The bipolar properties could be appear in right side of head (i.e. channels F8, FC6, C4, CP6, P8 and T8) and left side of head (i.e. channels F8, FC6, C4, CP6, P8 and T8) or frontal (i.e. Fp1, Fp2, F7, F3, Fz, F4, and F8) and posterior (i.e. P7, P3, P4, P8, O1, Oz, and O2) sides of the head. BCG artifacts contain fairly large peaks, as shown in Fig. 4(b) and have high energy. Removing such ICs effectively reduces BCG artifacts.

2.4.3. Muscle and residual imaging artifacts detection

Although the RecView is used to reduce imaging and BCG artifacts before applying ICA, some residual artifacts remain. Residual imaging and muscle artifacts are primarily distinguished based on power spectra with broad peaks at higher frequencies (i.e., higher than regular EEG signal) (McMenamin et al., 2010). Because such artifacts could appear in the beta band, only ICs with high frequency activity at 30 Hz and higher are considered muscle and imaging artifacts (See Fig. 4(c)). After reducing such artifacts, most sharp spikes with high amplitudes are removed from the EEG signal.

2.4.4. Motion artifact detection

Head, body, or electrode movement artifacts are easily recognized offline as a result of their large amplitude. Intervals containing these artifacts can be excluded without difficulty, given that such activity does not occur frequently for most subjects. Real-time analysis of such data is difficult because of the random nature of motion artifacts. Motion artifact ICs are characterized by high kurtosis values (of the order of 10–1000), intense low-frequency activity (0.5–4.5 Hz) and bipolar topographies similar to BCG artifacts with different threshold values (Wong et al., 2016; Zotev et al., 2012). Because of the large magnitude of the random-motion artifacts, they may appear across multiple ICs in the ICA decomposition. Removing movement artifacts may remove some brain activity as well. To prevent this, the number of IC-detected movement artifacts is limited to only those components with very large energy and kurtosis, as well as those with low frequency activity. Fig. 4(d) shows IC identified as motion artifacts, as well as the outcomes after removing them.

2.5. Implementation

The proposed algorithm was implemented in MATLAB (MathWorks Inc., Natick, MA) for offline testing. The SOBI algorithm, implemented in EEGLAB (Delorme and Makeig, 2004) was used for ICA decomposition.

For real-time implementation, software code was written in Python programming language as an add-on module for simultaneous rtfMRI-EEG neurofeedback system as described in Zotev et al. (2014). Real-time ICA decomposition of RecView-corrected EEG data was added to the EEG client software for removing artifacts from signals before performing Math modules and integrating EEG and fMRI. This processing module was named "eeg_rtica". Module outputs were saved to files in real time for further comparison with RecView-corrected data and offline methods.

2.6. Offline procedure for removing artifacts for evaluating rtAAS + rtICA algorithm

The BrainVision Analyzer 2 software (Brain Products GmbH, Germany) was used for offline analysis of the EEG data recorded simultaneously with fMRI. Different studies show that ICA following either the AAS or the OBS algorithms can successfully remove residual artifacts (Debener et al., 2008; Mantini et al., 2007; Zotev et al., 2014, 2016). Accordingly, for this study we primarily used this method as a reference to evaluate the rtAAS + rtICA performance and compare it with others. The procedure for offline EEG artifact removal using the AAS, filtering and ICA (AAS + Filtering + ICA) is the following. First, imaging artifacts were removed using the AAS method (Allen et al., 2000). EEG signals were then down-sampled to 250 S/s. Next, band-rejection filters (1 Hz bandwidth) were used for removing fMRI slice selection fundamental frequency (17 Hz) and its harmonics, vibration noise (26 Hz), and AC power line noise (60 Hz). These band-rejection filters should be selected based on the MRI scanner and sequence properties. For removing signals unrelated to brain activity, EEG data were bandpass filtered from 0.1 to 80 Hz (48 dB/octave). For detecting R-peaks more easily, ECG data were bandpass filtered from 0.1 to 12 Hz. Subsequently, BCG artifacts were removed using the AAS (Allen et al., 1998). A template of BCG artifacts from 21 cardiac periods of preceding data for each channel was used to create a template for removing BCG artifact using the AAS. Notably, R-peak detection is required for generating the BCG template. This can be accomplished automatically in the BrainVision Analyzer 2 software, with subsequent visual inspection to correct incorrectly positioned R-peak markers. After applying the AAS for reducing BCG artifacts, the Infomax algorithm (Bell and Sejnowski, 1995) was used for ICA decomposition. We chose the Infomax as ICA algorithm since this method is widely used for separating artifacts from EEG data and has been proven to be among the most reliable ICA methods for removing EEG artifacts (Nakamura et al., 2006; Vanderperren et al., 2010). However, we did not use this method for our rtICA implementation, because the Infomax is too slow for our real-time application (Klemm et al., 2009). ICA was performed on 31 channels, resulting in 31 ICs. The topographic map, power spectrum density, time course signal, energy value, and kurtosis value were used for detecting and removing artifactual ICs. Afterwards, EEG signal was reconstructed using inverse ICA. Furthermore, we compared the performance of the rtAAS + rtICA with two other offline artifact correction methods, consisting of removing imaging artifacts using the AAS, reducing imaging artifacts using AAS and other artifacts by means of our proposed automatic ICA-based method (this method was implemented offline, but it can be applied real-time as well). Finally, the rtAAS + rtICA results were compared with the RecView-corrected EEG data with imaging and BCG artifacts reduced in real time using the AAS.

2.7. Evaluation measures

Various evaluation metrics were used to determine the ability of the rtAAS + rtICA to reduce EEG artifacts (and, more importantly, preserve brain activity) and to compare its efficiency with that of offline correction.

2.7.1. The percentages of corrected eye blinks detected

To evaluate the algorithm performance for detecting eye blinks, EEG data were manually inspected to detect eye blinks and compare results to automatically detected eye blinks using the rtICA.

2.7.2. Power spectral density

To evaluate the rtAAS + rtICA performance given non-ideal conditions, we computed power spectral density (PSD) for all 22 EEG

Table 3
Eye blink detection results for 6 healthy subjects during eyes open resting state runs.

	Number of Eye Blinks Detected	True Number of Eye Blinks	Percentage of Eye Blinks Detected
Subject 1	190	193	98.45%
Subject 2	245	250	98.57%
Subject 3	82	84	97.62%
Subject 4	143	145	98.62%
Subject 5	71	75	94.67%
Subject 6	427	430	98.66%

channels before and after applying different artifact correction methods.

2.7.3. INPS reduction

To quantify changes and corrected improvements of BCG artifacts, the following Normalized Power Spectrum ratio (INPS) was computed as (Srivastava et al., 2005; Tong et al., 2001):

$$INPS = \frac{\Sigma_{i=1}^{N} PSD_i^{before\ BCG\ reduction}}{\Sigma_{i=1}^{N} PSD_i^{after\ BCG\ reduction}} \quad (4)$$

where N is the number of harmonics of ECG and PSD_i is the power spectral density of the ith ECG harmonic.

2.7.4. Power reduction in motion traces

Motion artifacts affect power spectrum significantly. To determine the efficiency of the rtAAS + rtICA for reducing such artifacts, we compared the power between 0.488 and 40.039 Hz using different algorithm in traces which were contaminated with motion artifacts.

3. Results

Fig. 5 shows a 4 s long segment of RecView-corrected EEG data (i.e., 22 channels) acquired simultaneously with fMRI, as well as the same trace of raw EEG recordings after removing imaging artifacts, rtAAS + rtICA corrected signal, AAS for imaging artifacts and automatic ICA corrected EEG data, and, finally, the clean EEG data using the proposed offline procedure.

Fig. 6 shows 22 ICs retrieved from RecView-corrected data with SOBI using equivalent traces presented in Fig. 5. In this example, IC 2, 5, and 6 were identified as eye artifact; IC 1, 3, and 7 were classified as residual BCG artifact; and IC22 were determined as a vibration noise at 26 Hz.

Table 3 shows the number of eye blinks detected using automatic rtICA method, as well as the number of actual blinks. Also detailed is the percentage of correctly detected eye blinks for the second and fourth runs (i.e. eyes open runs) for the six healthy subjects. The results demonstrate that rtICA effectively removes eye blink artifacts. Accurately detected eye blinks for all subjects were more than 94%.

Fig. 7 compares the performance of the BrainVision rtAAS, the rtAAS + rtICA and the offline methods in terms of INPS ratio. The INPS ratios for artifact correction methods were computed with respect to the EEG data obtained after removing imaging artifacts via offline AAS.

Fig. 8 demonstrates that, for most subjects, the rtAAS could not reduce effects of motion artifact on power value. However, the rtAAS + rtICA and the offline automatic ICA can reduce power during motion traces and can make it approximate the power value based on the offline AAS + Filtering + ICA artifact correction. The rtICA can significantly reduce effect of motion artifacts in all subjects.

Fig. 9 provides an example of the power spectral density of EEG data for a subject during eyes closed run using various artifact removal algorithms and shows that the rtAAS + rtICA can effectively reduce artifacts in different EEG frequency bands without affecting the neuronal alpha and beta activities.

Finally, Fig. 10 illustrates the power in several EEG bands before and after artifact correction. From Fig. 10(a), it can be observed that, for all subjects, the RecView-corrected EEG data have the highest power value in the delta frequency band when compared to the rtAAS + rtICA and two other artifact correction methods. The rtAAS + rtICA and offline automatic ICA methods reduce this power and make it approximate the EEG data after using the AAS + Filtering + ICA artifact correction. Notably, the delta power reflected mostly ocular and motion artifacts. Fig. 10(b) demonstrates theta power of corrected EEG data using a number of algorithms. BCG artifacts affect the theta band power. Again, the rtAAS + rtICA can reduce artifacts more effectively than only the rtAAS and the offline automatic ICA. Muscle and residual imaging artifacts primarily affect amplitude of power spectrum in the beta frequency band. It is critical that the rtICA algorithm not mistakenly remove brain activity, a significant portion of which is reflected in the alpha band power, shown in Fig. 10(c). The figure illustrates that even though the alpha power value was reduced using the rtAAS + rtICA and offline automatic ICA, the value does not dip below alpha power using the offline AAS + Filtering + ICA artifact correction. This amount serves as our reference for nearly-artifact-free EEG data. Furthermore, Fig. 10(c) and (d) demonstrate that without the rtAAS, the rtICA performs poorly when used to reduce effects of artifacts on the alpha and beta frequency bands. From Fig. 10(d), we can observe that the rtAAS + rtICA could more effectively reduce such artifacts when compared to the performance of the rtAAS and rtICA.

4. Discussion

Few methods have been developed for real-time removal of BCG and imaging artifacts from EEG data recorded during fMRI. This has limited the application of real-time EEG-fMRI systems. We propose a novel algorithm based on ICA for attenuating all types of artifact in EEG data acquired during fMRI scans. The proposed real-time ICA method can further be utilized for any application requiring real-time ICA decomposition.

Although the rtAAS is supposed to reduce BCG artifacts, we can see in Fig. 7 that the average INPS value is less than zero for two subjects when using the rtAAS. Averaging the INPS among six subjects shows 4.4 times larger INPS reduction was achieved by using rtAAS + rtICA compared to rtAAS. For subject 1, the enormous amount of motion artifacts prevents the RecView from performing well. Furthermore, the ECG signal from subjects 1 and 4 are severely distorted, which makes detecting R-peak and creating accurate BCG artifact template in real time impossible. Except for subject 4, INPS reduction by the rtAAS + rtICA and offline automatic ICA is comparable with that of the AAS + Filtering + ICA method. The poor performance of the rtAAS + rtICA in terms of INPS for subject 4 could be the result of the low performance of the rtAAS.

Eye blink, motion and muscle artifacts are problematic and obscure the EEG signal quality significantly, but so far, there is no robust real-time method for removing such artifacts. The results of removing such artifacts in Table 3, Figs. 8 and 10(d) show that the rtICA can substantially reduce effects of these artifacts on EEG signal.

Based on evaluation metrics, the rtAAS + rtICA has superior performance when compared to the rtAAS and the rtICA. One reason for this phenomenon is that either the ICA or AAS might not effectively reduce BCG and imaging artifacts for some subjects. Thus, both methods complement each other when removing imaging, BCG, and other artifacts.

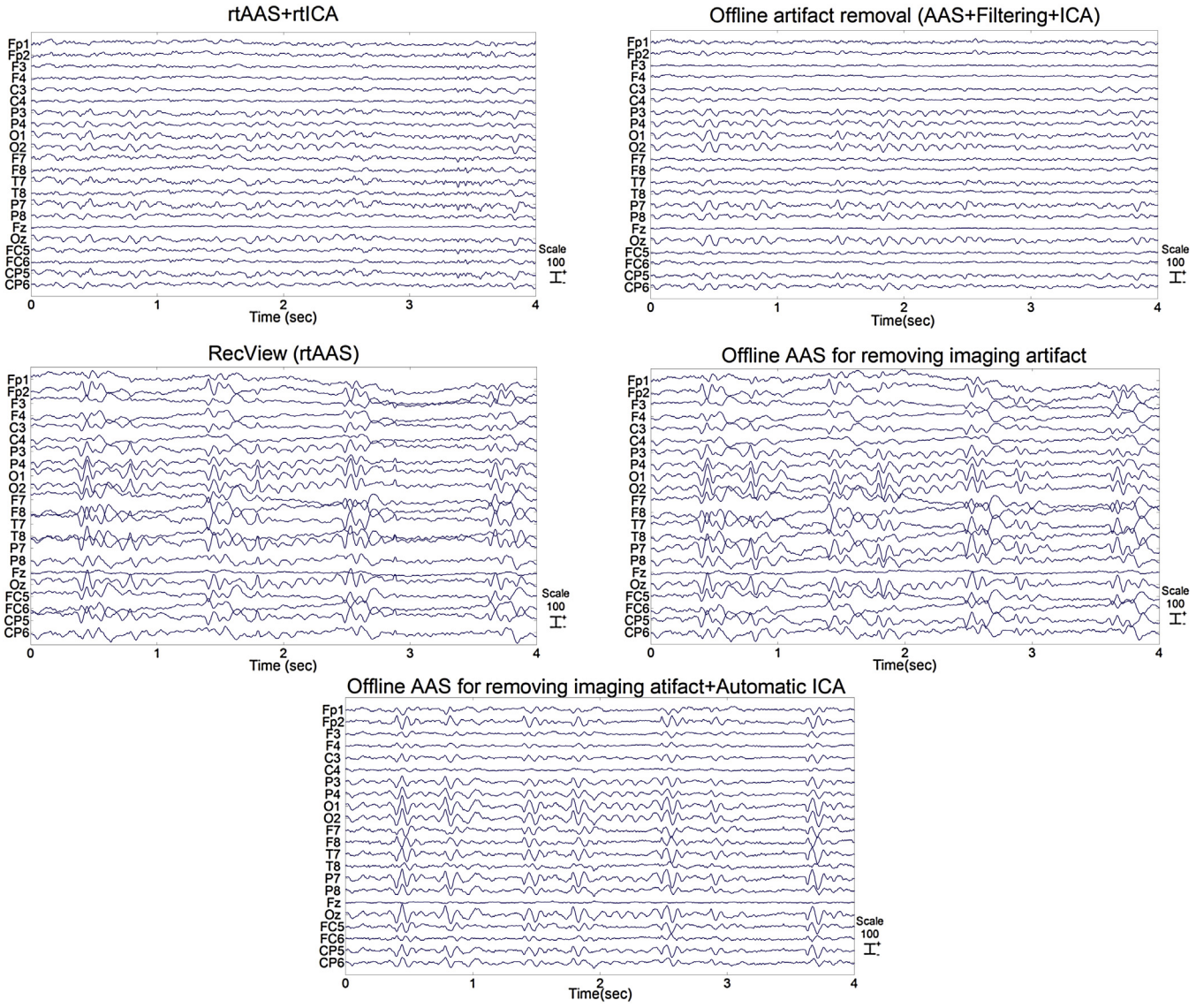

Fig. 5. Representative 4-s example traces of EEG data recorded during fMRI acquisition (subject 4 during eyes open run) after applying different offline and real-time artifact correction methods.

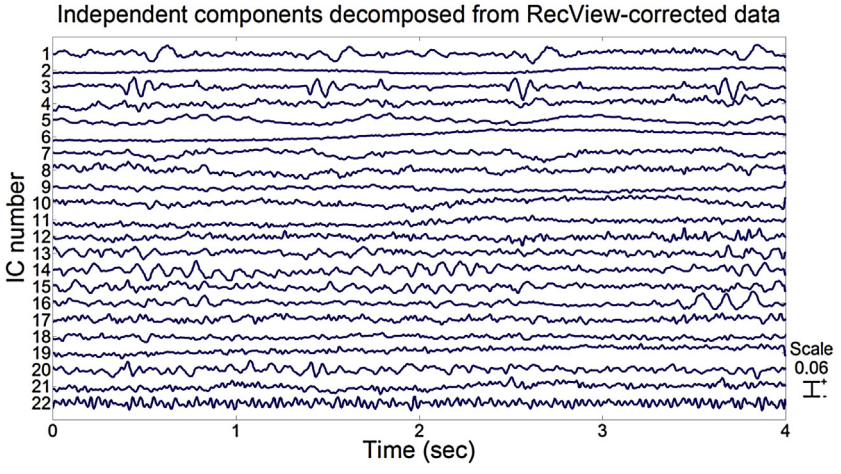

Fig. 6. 22 ICs decomposed from 22 channels RecView-corrected EEG data (the same trace as Fig. 5) using rtICA in real time.

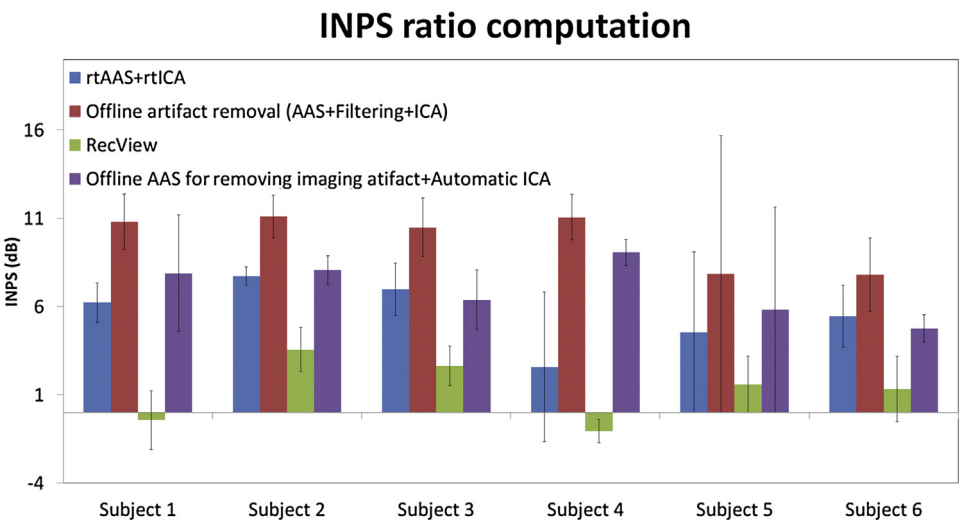

Fig. 7. INPS Reduction for all channels using different artifact correction methods versus the EEG data after removing imaging artifacts.

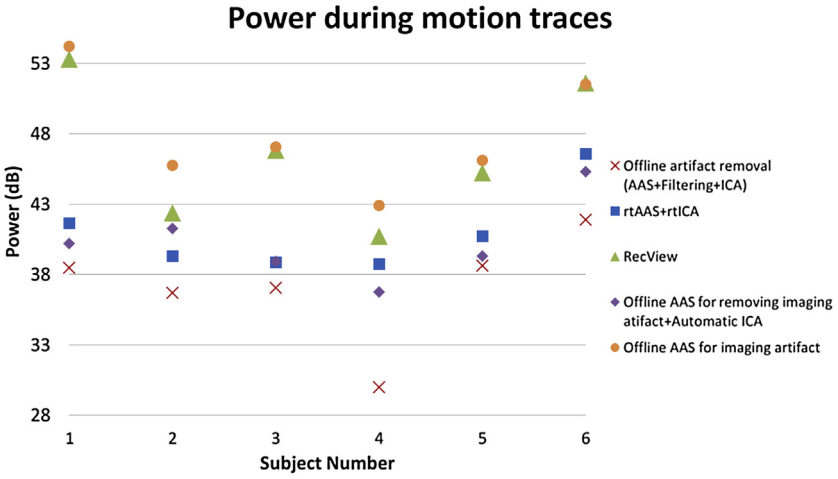

Fig. 8. Compression of power during motion traces using AAS + rtICA, RecView and offline artifact correction methods with power without any correction (EEG data after applying AAS for imaging artifact correction).

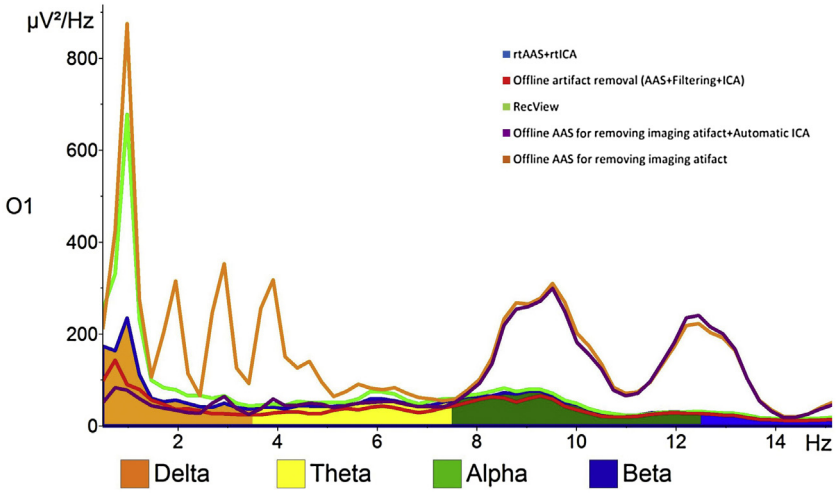

Fig. 9. An example of power spectral density of electrode O1 (for subject 2) during eyes-closed runs using different artifact removal algorithms.

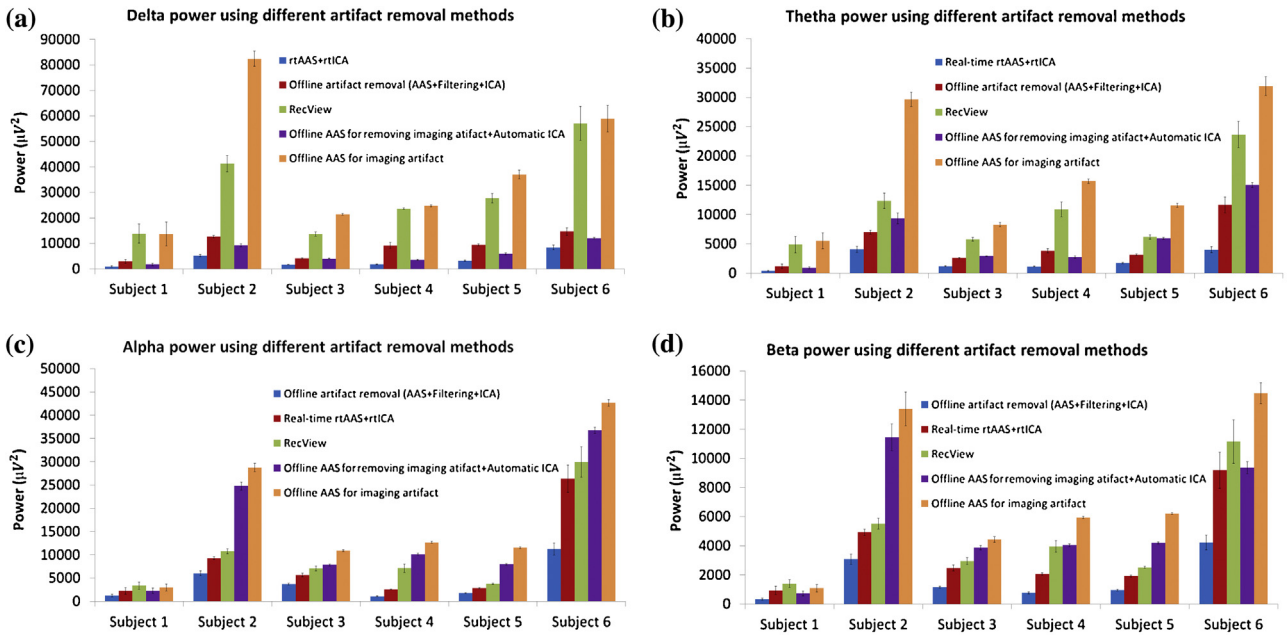

Fig. 10. The impact of different artifact correction on EEG power in (a) delta (b) theta (c) alpha and (d) beta frequency bands. Bar heights represent averages across channels, and error bars represent the standard error across ICA windows. Results are shown for all 6 subjects using average data from all 22 channels and all 4 resting state runs.

It is likely that our proposed real-time technique might not perform as efficiently as offline artifact detection techniques. Admittedly, several factors can lessen the method efficiency and can be further optimized. The most important factor is the accuracy of the real-time IC classification that separates various artifacts from the ICs describing neuronal activity. The classification criteria and numerical threshold settings used in this work will need to be optimized and refined further. For instance, recording test data before starting the actual experiment and using the test data as an input for a machine learning algorithm for classifying brain activity and artifact ICs may improve the efficiency of the method. Using mutual information appears helpful in this regard (Abbasi et al., 2015; Liu et al., 2012).Another important factor is the algorithm speed. When the algorithm is implemented in MATLAB, less than 1 s is required for removing artifacts from 4 s of EEG data; between 2 s and 4 s is required for this when running our stand-alone and proof-of-concept software implementation written in Python. Performing the ICA decomposition using the SOBI requires the greatest amount of time. Thus, implementing this particular code (i.e., ICA decomposition using the SOBI) in Cython (Behnel et al., 2011) or assisting C might aid in speeding up the algorithm. By increasing the method speed, we can apply ICA on 31 channels instead of 22 channels. This could improve the performance of the method for artifact correction. The recent study demonstrates that Online Recursive ICA (ORICA) can be successfully implemented in real time for source separation, but more investigations are needed to evaluate the ORICA efficiency for distinguishing ICs related to artifacts from brain activities (Hsu et al., 2016). Even though still there are opportunities to speed up the algorithm, the method can be used for real-time neurofeedback application and real-time monitoring of brain activity since the rtICA updates EEG results in the comparable time with fMRI (which is equal to TR).

5. Conclusion

Recording EEG during fMRI acquisition leads to EEG data contamination with large fMRI environment artifacts. Most EEG-fMRI studies have reduced artifacts offline; however only a few have involved real-time correction. We have introduced ICA-based real-time EEG artifact correction during fMRI. This novel approach was successfully implemented and improved real-time EEG artifacts detection and removal during fMRI on all 6 healthy subjects. The proposed algorithm can be effectively implemented for various applications that require a real-time EEG signal with artifacts suppressed (e.g., neurofeedback and online monitoring of brain activity). Our work represents an important first step towards a wider use of ICA methods in real-time EEG-fMRI applications, such as determining the (functional) neural correlates of the EEG rhythms used in rtEEG neurofeedback and rtfMRI data.

Acknowledgment

This work was supported by the U.S. Department of Defense grant W81XWH-12-1-0607.

References

Abbasi, O., Dammers, J., Arrubla, J., Warbrick, T., Butz, M., Neuner, I., Shah, N.J., 2015. Time-frequency analysis of resting state and evoked EEG data recorded at higher magnetic fields up to 9.4 T. J. Neurosci. Methods 255, 1–11.

Akhtar, M.T., Mitsuhashi, W., James, C.J., 2012. Employing spatially constrained ICA and wavelet denoising for automatic removal of artifacts from multichannel EEG data. Signal Process. 92, 401–416.

Allen, P.J., Polizzi, G., Krakow, K., Fish, D.R., Lemieux, L., 1998. Identification of EEG events in the MR scanner: the problem of pulse artifact and a method for its subtraction. Neuroimage 8, 229–239.

Allen, P.J., Josephs, O., Turner, R., 2000. A method for removing imaging artifact from continuous EEG recorded during functional MRI. Neuroimage 12, 230–239.

Bénar, C.G., Aghakhani, Y., Wang, Y., Izenberg, A., Al-Asmi, A., Dubeau, F., Gotman, J., 2003. Quality of EEG in simultaneous EEG-fMRI for epilepsy. Clin. Neurophysiol. 114, 569–580.

Becker, R., Ritter, P., Villringer, A., 2008. Influence of ongoing alpha rhythm on the visual evoked potential. Neuroimage 39, 707–716.

Becker, R., Reinacher, M., Freyer, F., Villringer, A., Ritter, P., 2011. How ongoing neuronal oscillations account for evoked fMRI variability. J. Neurosci. 31, 11016–11027.

Behnel, S., Bradshaw, R., Citro, C., Dalcin, L., Seljebotn, D.S., Smith, K., 2011. Cython: the best of both worlds. Comput. Sci. Eng. 13, 31–39.

Bell, A.J., Sejnowski, T.J., 1995. An information-maximization approach to blind separation and blind deconvolution. Neural Comput. 7, 1129–1159.

Belouchrani, A., Abed-Meraim, K., Cardoso, J.-F., Moulines, E., 1997. A blind source separation technique based on second-order statistics. IEEE Trans. Signal Process. 45, 434–444.

Bonmassar, G., Purdon, P.L., Jääskeläinen, I.P., Chiappa, K., Solo, V., Brown, E.N., Belliveau, J.W., 2002. Motion and ballistocardiogram artifact removal for interleaved recording of EEG and EPs during MRI. Neuromage 16, 1127–1141.
Cavazza, M., Aranyi, G., Charles, F., Porteous, J., Gilroy, S., Klovatch, I., Jackont, G., Soreq, E., Keynan, N.J., Cohen, A., Raz, G., Hendler, T., 2014. Towards empathic neurofeedback for interactive storytelling. OpenAccess Ser. Inform. 41, 42–60.
Debener, S., Mullinger, K.J., Niazy, R.K., Bowtell, R.W., 2008. Properties of the ballistocardiogram artifact as revealed by EEG recordings at 1.5, 3 and 7 T static magnetic field strength. Int. J. Psychophysiol. 67, 189–199.
Delorme, A., Makeig, S., 2004. EEGLAB: an open source toolbox for analysis of single-trial EEG dynamics including independent component analysis. J. Neurosci. Methods 134, 9–21.
Dunseath, W.J.R., Alden, T.A., 2010. Apparatus and method for acquiring a signal. U.S. Patent 7715894.
Hsu, S., Mullen, T.R., Jung, T., Cauwenberghs, G., 2016. Real-time adaptive EEG source separation using online recursive independent component analysis. IEEE Trans. Neural Syst. Rehabil. Eng. 24, 309–319.
Jorge, J., Grouiller, F., Gruetter, R., Van Der Zwaag, W., Figueiredo, P., 2015. Towards high-quality simultaneous EEG-fMRI at 7 T: detection and reduction of EEG artifacts due to head motion. Neuroimage 120, 143–153.
Kim, K.H., Yoon, H.W., Park, H.W., 2004. Improved ballistocardiac artifact removal from the electroencephalogram recorded in fMRI. J. Neurosci. Methods 135, 193–203.
Klemm, M., Haueisen, J., Ivanova, G., 2009. Independent component analysis: comparison of algorithms for the investigation of surface electrical brain activity. Med. Biol. Eng. Comput. 47, 413–423.
Kruggel, F., Wiggins, C.J., Herrmann, C.S., von Cramon, D.Y., 2000. Recording of the event-related potentials during functional MRI at 3.0 T field strength. Magn. Reson. Med. 44, 277–282.
Laufs, H., 2012. A personalized history of EEG-fMRI integration. Neuroimage 62, 1056–1067.
Liu, Z., de Zwart, J.A., van Gelderen, P., Kuo, L.W., Duyn, J.H., 2012. Statistical feature extraction for artifact removal from concurrent fMRI-EEG recordings. Neuroimage 59, 2073–2087.
Luo, Q., Huang, X., Glover, G.H., 2014. Ballistocardiogram artifact removal with a reference layer and standard EEG cap. J. Neurosci. Methods 233, 137–149.
Mantini, D., Perrucci, M.G., Cugini, S., Ferretti, A., Romani, G.L., Del Gratta, C., 2007. Complete artifact removal for EEG recorded during continuous fMRI using independent component analysis. Neuroimage 34, 598–607.
Masterton, R.A.J., Abbott, D.F., Fleming, S.W., Jackson, G.D., 2007. Measurement and reduction of motion and ballistocardiogram artefacts from simultaneous EEG and fMRI recordings. Neuroimage 37, 202–211.
Mayeli, A., Zotev, V., Refai, H., Bodurka, J., 2015. An automatic ICA-based method for removing artifacts from EEG data acquired during fMRI in real time. IEEE 41st Annual Northeast Biomedical Engineering Conference (NEBEC).
McMenamin, B.W., Shackman, A.J., Maxwell, J.S., Bachhuber, D.R.W., Koppenhaver, A.M., Greischar, L.L., Davidson, R.J., 2010. Validation of ICA-based myogenic artifact correction for scalp and source-localized EEG. Neuroimage 49, 2416–2432.
Nakamura, W., Anami, K., Mori, T., Saitoh, O., Cichocki, A., Amari, S., 2006. Removal of ballistocardiogram artifacts from simultaneously recorded EEG and fMRI data using independent component analysis. IEEE Trans. Biomed. Eng. 53, 1294–1308.
Negishi, M., Abildgaard, M., Nixon, T., Constable, R.T., 2004. Removal of time-varying gradient artefacts during continuous fMRI. Clin. Neurophysiol. 115, 2181–2192.
Niazy, R.K., Beckmann, C.F., Iannetti, G.D., Brady, J.M., Smith, S.M., 2005. Removal of FMRI environment artifacts from EEG data using optimal basis sets. Neuroimage 28, 720–737.
Onton, J., Westerfield, M., Townsend, J., Makeig, S., 2006. Imaging human EEG dynamics using independent component analysis. Neurosci. Biobehav. Rev. 30, 808–822.
Ritter, P., Villringer, A., 2006. Simultaneous EEG-fMRI. Neurosci. Biobehav. Rev. 30, 823–838.
Srivastava, G., Crottaz-Herbette, S., Lau, K.M., Glover, G.H., Menon, V., 2005. ICA-based procedures for removing ballistocardiogram artifacts from EEG data acquired in the MRI scanner. Neuroimage 24, 50–60.
Tong, S., Bezerianos, A., Paul, J., Zhu, Y., Thakor, N., 2001. Removal of ECG interference from the EEG recordings in small animals using independent component analysis. J. Neurosci. Methods 108, 11–17.
van der Meer, J.N., Pampel, A., Van Someren, E.J., Ramautar, J.R., van der Werf, Y.D., Gomez-Herrero, G., Lepsien, J., Hellrung, L., Hinrichs, H., Möller, H.E., Walter, M., 2016. Carbon-wire loop based artifact correction outperforms post-processing EEG/fMRI corrections—a validation of a real-time simultaneous EEG/fMRI correction method. Neuroimage 125, 880–894.
Vanderperren, K., De Vos, M., Ramautar, J.R., Novitskiy, N., Mennes, M., Assecondi, S., Vanrumste, B., Stiers, P., Van den Bergh, B.R., Wagemans, J., Lagae, L., Sunaert, S., Van Huffel, S., 2010. Removal of BCG artifacts from EEG recordings inside the MR scanner: a comparison of methodological and validation-related aspects. Neuroimage 50, 920–934.
Wong, C.K., Zotev, V., Misaki, M., Phillips, R., Luo, Q., Bodurka, J., 2016. Automatic EEG-assisted retrospective motion correction for fMRI (aE-REMCOR. Neuroimage 129, 133–147.
Wu, X., Wu, T., Zhan, Z., Yao, L., Wen, X., 2016. A real-time method to reduce ballistocardiogram artifacts from EEG during fMRI based on optimal basis sets (OBS). Comput. Methods Progr. Biomed. 127, 114–125.
Yuan, H., Zotev, V., Phillips, R., Bodurka, J., 2013. Correlated slow fluctuations in respiration, EEG, and BOLD fMRI. Neuroimage 79, 81–93.
Zhou, W., Gotman, J., 2004. Removal of EMG and ECG artifacts from EEG based on wavelet transform and ICA. Conference Proceedings. IEEE Engineering in Medicine and Biology Society, 392–395.
Zich, C., Debener, S., Kranczioch, C., Bleichner, M.G., Gutberlet, I., De Vos, M., 2015. Real-time EEG feedback during simultaneous EEG-fMRI identifies the cortical signature of motor imagery. Neuroimage 114, 438–447.
Zotev, V., Yuan, H., Phillips, R., Bodurka, J., 2012. EEG-assisted retrospective motion correction for fMRI: E-REMCOR. Neuroimage 63, 698–712.
Zotev, V., Phillips, R., Yuan, H., Misaki, M., Bodurka, J., 2014. Self-regulation of human brain activity using simultaneous real-time fMRI and EEG neurofeedback. Neuroimage 85, 985–995.
Zotev, V., Yuan, H., Misaki, M., Phillips, R., Young, K.D., Feldner, M.T., Bodurka, J., 2016. Correlation between amygdala BOLD activity and frontal EEG asymmetry during real-time fMRI neurofeedback training in patients with depression. Neuroimage: Clin. 11, 224–238.